Escherichia coli O176 LPS structure and dynamics: A NMR spectroscopy and MD simulation study

Dhilon S. Patel [a],[1], Pilar Blasco [b],[1], Göran Widmalm [b],[**], Wonpil Im [a],[*]

[a] *Departments of Biological Sciences, Chemistry, and Bioengineering, Lehigh University, Bethlehem, PA, 18015, USA*
[b] *Department of Organic Chemistry, Arrhenius Laboratory, Stockholm University, SE-106 91, Stockholm, Sweden*

A B S T R A C T

A lipopolysaccharide (LPS) molecule is a key component of the bacterial outer membrane used to protect the bacterium and to interact with the environment. To gain insight into its function, the study of the LPS conformation and dynamics at the molecular and cellular levels is necessary, but these highly diverse and dynamic membrane-LPS systems are difficult to study. In this work, by using NMR spectroscopy and molecular dynamics (MD) simulations, we determined the conformational preferences of an *E. coli* O176 O-antigen polysaccharide at the atomic level. Moreover, we analyzed the use of non-uniform sampling (NUS) for the acquisition of high dynamic range spectra, like ^{1}H,^{1}H-NOESY NMR experiments. A comparison of the effective transglycosidic distances derived from conventional uniformly sampled and NUS ^{1}H,^{1}H-NOESY data showed high similarity under equal measuring time conditions. Furthermore, the experimentally derived internuclear distances of the O-antigen polysaccharide with ten repeating units (RUs) showed very good agreement to those calculated from the MD simulations of the same O-antigen polysaccharide in solution. Analysis of the LPS bilayer simulations with five and with ten RUs revealed that, although similar with respect to populated states in solution, the O-antigen in LPS bilayers had more extended chains as a result of spatial limitations due to close packing. Additional MD simulations of O-antigen polysaccharides from *E. coli* O6 (branched repeating unit) and O91 (negatively charged linear repeating unit) in solution and LPS bilayers were performed and compared to those of O176 (linear polymer). For all three O-antigens, the ensemble of structures present for the polysaccharides in solution were consistent with the results from their ^{1}H,^{1}H-NOESY experiments. In addition, the similarities between the O-antigen on its own and as a constituent of the full LPS in bilayer environment makes it possible to realistically describe the LPS conformation and dynamics from the MD simulations.

1. Introduction

Carbohydrates are the most abundant organic molecules in nature; all living organisms are able to synthesize carbohydrates and metabolize them (Wade, 1999). These molecules are involved in many biological processes, like protein folding, oligomerization and stability, immune response, and host-pathogen interactions (Varki, 2017). The high complexity found in glycan modifications gives an immense repertoire of biological information that is not encoded in the genome (Feizi and Mulloy, 2003). Glycans can be attached to proteins forming glycoproteins or proteoglycans (Prestegard et al., 2015), but also linked to lipids (glycolipids) or even forming free polymers (e.g., hyaluronic acid) in the extracellular space. Their structural diversity resides in the type of linkages, variation of functional groups, stereoisomers, length, branching pattern, and sequence order (Woods, 2018). Moreover, not only the primary sequence, but also the polysaccharide spatial behavior in its cellular context have been found essential to function. Therefore,

knowledge of the three-dimensional structure and conformational preferences in their environment is crucial in order to understand their roles at a molecular level.

A lipopolysaccharide (LPS) molecule is the major component of the outer membrane in gram-negative bacteria. Bacteria use LPS to interact with the environment, from attachment to inorganic materials to aggregation with other cells (Alexander and Rietschel, 2001). A LPS molecule consists of a conserved lipid-carbohydrate moiety termed lipid A that is anchored in the outer bacterial membrane, the core region that is covalently linked to lipid A and can be divided into the outer and inner cores, and an O-antigen polysaccharide region that is linked to the outer core (Ståhle and Widmalm, 2019). The negative charges of the core oligosaccharide and lipid A generate strong ionic interactions with divalent cations, which is crucial for the membrane integrity and structure stabilization (Rietschel et al., 1994). The O-antigen is a polymer with 2–7 monosaccharides per repeating unit (RU), arranged into linear or branched structures. More complex three-dimensional

* Corresponding author.
** Corresponding author.
   E-mail addresses: goran.widmalm@su.se (G. Widmalm), wonpil@lehigh.edu (W. Im).
[1] Equal contribution.

structures can be formed when the number of branches increases. Moreover, the O-antigen polysaccharide has various RU lengths, and its composition and structure vary according to the serological group (Stenutz et al., 2006).

The combination of NMR relaxation measurements and molecular dynamics (MD) simulations has been used in the study of carbohydrate conformations in solution (Boutet et al., 2016; Landersjö et al., 2005; Pendrill et al., 2013; Wu et al., 2013). To better understand its function, it is necessary to study the LPS structure, conformation, and dynamics at the molecular level as well as in its cellular environment. However, simulations of complex systems like LPS in membrane environments (Enkavi et al., 2019) have been limited because of the difficulty in building membrane-LPS models (Jo et al., 2015), and the lack of appropriate molecular force fields. We have successfully developed a protocol to build LPS bilayers (Lee et al., 2019) by using CHARMM (Brooks et al., 2009) and the modified CHARMM-GUI *Membrane Builder* procedure for lipoglycans, which was applied for the study of the dynamics of the LPS from *E. coli* O6 and O91. In the case of *E. coli* serotype O6 (Fig. 1, →4)-α-D-GalpNAc-(1 → 3) [β-D-Glcp-(1 → 2)]-β-D-Manp-(1 → 4)-β-D-Manp-(1 → 3)-α-D-GalpNAc-(1→)), the effective proton-proton distances in the polysaccharide were analyzed from NMR experiments and MD simulations using lipid bilayers (Wu et al., 2013). Moreover, for *E. coli* serotype O91 (Fig. 1, →4)-α-D-Quip-3-*N*-[(*R*)-3-hydroxybutyramido]-(1 → 4)-β-D-Galp-(1 → 4)-β-D-GlcpNAc-(1 → 4)-β-D-GlcpA-6-*N*-Gly-(1 → 3)-β-D-GlcpNAc-(1→), the MD simulations could reproduce the dynamical behavior of NMR correlation times observed for the polysaccharide chain in solution (Blasco et al., 2017).
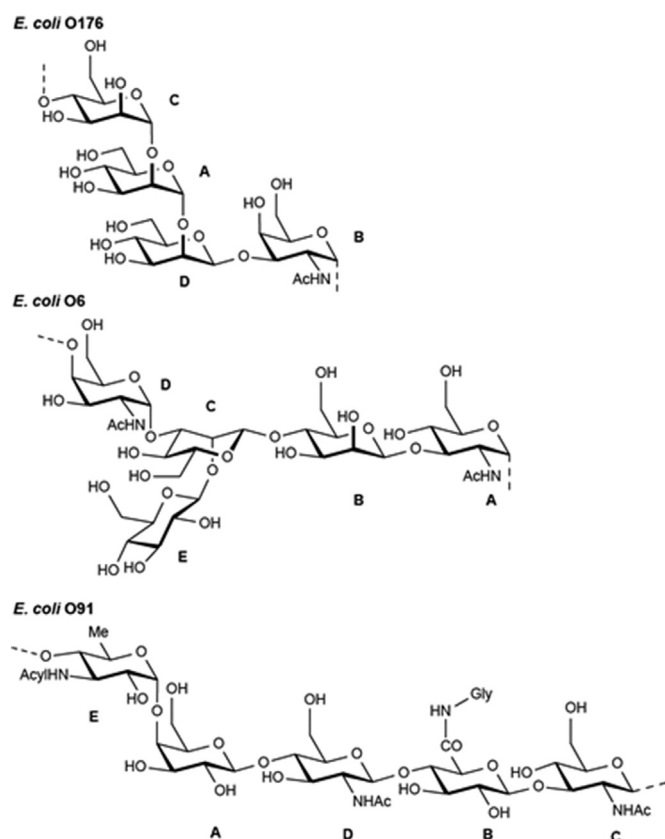

Fig. 1. Schematic structures of the repeating units of the O-antigen polysaccharides from *E. coli* O176 (top, linear repeating unit), O6 (middle, branched repeating unit), and O91 (bottom, negatively charged linear repeating unit), where the latter two are adapted from Wu et al. (Wu et al., 2013) and Blasco et al. (Blasco et al., 2017), respectively. Sugar residues are labeled by capital letters.

In this work, the conformational preferences of *E. coli* O176 O-antigen polysaccharide (Fig. 1, →4)-α-D-Manp-(1 → 2)-α-D-Manp-(1 → 2)-β-D-Manp-(1 → 3)-α-D-GalpNAc-(1→)) were determined at the atomic level by a combination of NMR spectroscopy and MD simulations. We analyzed the use of non-uniform sampling (Orekhov and Jaravine, 2011) for the acquisition of 2D ^{1}H,^{13}C-HSQC and ^{1}H,^{1}H-NOESY NMR experiments. Furthermore, the LPS structure and dynamics in a membrane environment were investigated. In particular, results from MD simulation trajectories of the *E. coli* O176 O-antigen containing 10 RUs (PS10) in solution were compared with those calculated from NMR experiments. Moreover, additional MD simulations of the O6 (branched) and O91 (linear, but negatively charged) polysaccharides were performed and compared to those of the (linear) O176 O-antigen.

2. Materials and methods

2.1. NMR experiments

The NMR experiments were performed on an *E. coli* O176 O-antigen polysaccharide preparation in D$_2$O using a natural abundance sample (16 mg in 0.50 mL); to this end, the material was treated with CHELEX-100 resin, filtered, and transferred to a 5 mm NMR tube. ^{1}H and ^{13}C NMR chemical shifts were referenced to external 3-trimethylsilyl-(2,2,3,3-^{2}H$_4$)-propanoate (TSP, δ_H = 0.00 ppm) and 1,4-dioxane in D$_2$O (δ_C = 67.40 ppm). ^{1}H and ^{13}C NMR chemical shift assignments were available from literature (Olsson et al., 2008).

A 600 MHz Bruker AVANCE III spectrometer was used for experiments at 313.15 K, where the temperature had been calibrated with a sample of neat deuterated methanol (Findeisen et al., 2007). Multiplicity-edited ^{1}H,^{13}C-HSQC experiments were performed with a 60 kHz smoothed Chirp pulse (0.5 ms, 20.1% smoothing) for the initial and final ^{13}C pulses of the pulse sequence and a broadband GARP4 ^{13}C-decoupling sequence. Spectra were acquired with 512 × 2k data points, spectral widths of 70 × 3 ppm in the F_1 and F_2 dimensions, respectively, and a relaxation delay of 5 s. Six experiments were carried out; one with the traditional uniform sampling (US) method using 512 data points and five with varying non-uniform sparse sampling (NUS, using 2, 5, 10, 20, and 40% sampling corresponding to 5, 13, 26, 51 and 102 data points recorded) employing a random sampling scheme to generate the different distribution of the data points (Kazimierczuk and Orekhov, 2015). NUS spectra were recorded with T_2 relaxation time set to 53 ms in the indirect dimension and a $^1J_{CH}$ of 150 Hz to give more weight to the parts of the FID (free induction decay) with higher intensity. Compressed sensing was used for reconstruction of the full data set prior to Fourier transformation (Kazimierczuk and Orekhov, 2011).

Phase-sensitive ^{1}H,^{1}H-NOESY experiments of the polysaccharide with zero-quantum coherence suppression (Thrippleton and Keeler, 2003) were performed with a relaxation delay of 10 s and acquired with 256 × 2k data points in the F_1 and F_2 dimensions and a spectral width of 6 ppm. Six spectra with 20, 25, 30, 35, 40, and 50% NUS were used for the sparseness estimation, and a NUS scheme with 40% coverage corresponding to a total 102 data points was finally chosen for further experiments. US and NUS (Mobli et al., 2012) spectra were recorded with eight mixing times varying from 60 to 180 ms (60, 80, 90, 100, 120, 140, 160, and 180 ms), where each mixing time was acquired in quintuplicate. US and NUS spectra were recorded using 16 and 40 scans per t_1-increment, respectively (2.5-fold difference), to equalize experimental time and compare cross relaxation rates between sampling methods. Peak volumes in the two-dimensional (2D) spectra were integrated for auto- and cross-peaks to construct NOE buildup curves (Hu and Krishnamurthy, 2006; Macur et al., 1986; Widmalm et al., 1992) followed by the PANIC approach, in which every cross-peak volume at each mixing time was divided by its corresponding auto-peak volume of the anomeric resonance. The fitting of the PANIC data by a first order function was used to calculate the cross-relaxation rates.

2.2. Analysis of NMR data

Proton-proton distances were obtained from cross-relaxation rates (σ) employing the isolated spin-pair approximation (ISPA) (Thomas et al., 1991). The set of reference distances (r_{ref}) was taken from the MD simulation of the O-antigen polysaccharide with ten RUs in solution (PS10; see below for the details), omitting the first and last RUs for the analysis. The value of $\sigma_{ref} \cdot r_{ref}^6$ was calculated for the available reference interactions (C1–C2, A1-A2, D1-D3, D1-D5, and B1–B2 where A, B, C, and D are four sugar residues in O176 RU and numbers are hydrogen numbers in each sugar; see Fig. 1) using effective distances from the MD simulations, and their average, $\sigma_{ref} \cdot r_{ref}^6$, was subsequently used to calculate r_{ij} according to $r_{ij}^6 = \sigma_{ref} \cdot r_{ref}^6 / \sigma_{ij}$ for the interaction between protons i and j for the US and NUS ^{1}H,^{1}H-NOESY experiments (Patel et al., 2014). The standard error of the slope (SES) was calculated for all cross-relaxation rates and distances. Errors in σ were calculated using the jackknife procedure (Efron and Stein, 1981) and are reported as one standard deviation (SD). Based on ± 1 SD, errors were subsequently estimated for the experimentally determined proton-proton distances. Constraints employed in the fitting procedure were that the y-axis intercept should be within 5% of the value at the longest mixing time and the correlation coefficient $R^2 > 0.9$. A final visual inspection of the PANIC plots reassured the quality of the fitting procedure.

2.3. Molecular dynamics simulations system setup

An initial polysaccharide conformation containing 10 RUs (PS10) was generated for each of the O-antigen O176, O6, and O91 using the topology information in the CHARMM force field (Patel et al., 2014; Guvench et al., 2008, 2009, 2011) and subjected to a brief energy minimization using steepest descent and adopted basis New-ton−Raphson methods. Two PS10 solution simulation systems for O176 O-antigen and three PS10 solution simulation systems for O6 and O91 O-antigens were built independently using *Glycan Reader & Modeler* in CHARMM-GUI (http://www.charmm-gui.org) (Jo et al., 2008, 2011; Park et al., 2019). The system size was determined to have at least a 12.5 Å water layer in every direction. The solution simulation systems were energy minimized with the positional harmonic restraints applied to the non-hydrogen atoms of PS10 using CHARMM simulation software (Brooks et al., 2009). The system size of each solvated PS10 system is given in Table S1.

For each of O-antigen O176, O6 and O91, building and assembly of two LPS bilayer systems LPS5 (lipid A + R1 core + 5 RUs of O-antigen) and LPS10 (lipid A + R1 core + 10 RUs of O-antigen) (Fig. 2) were achieved by the well-established step-by-step protocol in CHARMM-GUI *Membrane Builder* (Lee et al., 2019; Jo et al., 2007, 2008, 2009; Wu et al., 2014a,b) and successfully used in previous LPS simulations (Wu et al., 2013, 2014; Jo et al., 2015; Patel et al., 2016). For LPS5 and LPS10 bilayer systems containing 36 LPS molecules in each leaflet where each LPS molecule of O176 and O6 in LPS5 and LPS10 systems consist net charge of –9e where as in O91 LPS5 system there is net charge of –14e and O91 LPS10 system consist net charge of –19e. These highly negative LPS bilayer systems were neutralized with Ca^{2+} ions where initial placement of Ca^{2+} ions restricted to neutralize all the negative charges on the lipid A head groups and of the core sugar residues Kdo (2-keto-3-deoxyoctulosonate) and phosphorylated Hep (L-glycero-D-manno heptose). Ca^{2+} ions and additional 150 mM KCl bulk ions were placed using 2000 steps of Monte Carlo simulations. No extra bulk ions were added for PS10 solution systems. These building steps were repeated three times with different random seed numbers to generate three independent replicas to improve sampling and to check for simulation convergence. The system sizes of solvated LPS5 and LPS10 systems are given in Table S1.

2.4. Simulation protocols

The energy minimized solution systems for each of O176, O6 and O91 PS10 were subjected to 50-ps NVT (constant particle number, volume, and temperature) and NPT (constant particle number, pressure, and temperature) equilibration using CHARMM followed by 400-ns NAMD production simulations at 300 K. Similarly, LPS5 and LPS10 membrane systems were equilibrated for 450 ps using CHARMM (Brooks et al., 2009), where Langevin temperature control was used for NVT dynamics, and a Hoover thermostat (Hoover, 1985) and the Langevin piston methodology was used to control temperature and pressure for NPT dynamics (Andersen, 1980; Nosé and Klein, 1983). This was followed by 400-ns NPT production runs with NAMD (Phillips et al., 2005) using the NAMD input scripts generated by CHARMM-GUI (Lee et al., 2016). This resulted in a total simulation time of 1.2 μs for each PS10, LPS5, and LPS10 systems, except for 800 ns for the O176 PS10 system. During LPS5 and LPS10 equilibration, various planar and dihedral restraints were applied to the LPS molecules; these restraint forces were gradually reduced to zero for the production simulations (Wu et al., 2013, 2014). Additional dihedral angle restraints were applied to restrain all sugar rings to the pertinent chair conformation, which were maintained during the production simulations in both solution and membrane simulation systems. These restraints were used in our previous simulations (Wu et al., 2013, 2014; Jo et al., 2015; Patel et al., 2016). The temperature and pressure were held at 310.15 K and 1 bar, respectively, for the membrane systems. In NAMD production runs, Langevin dynamics was used to
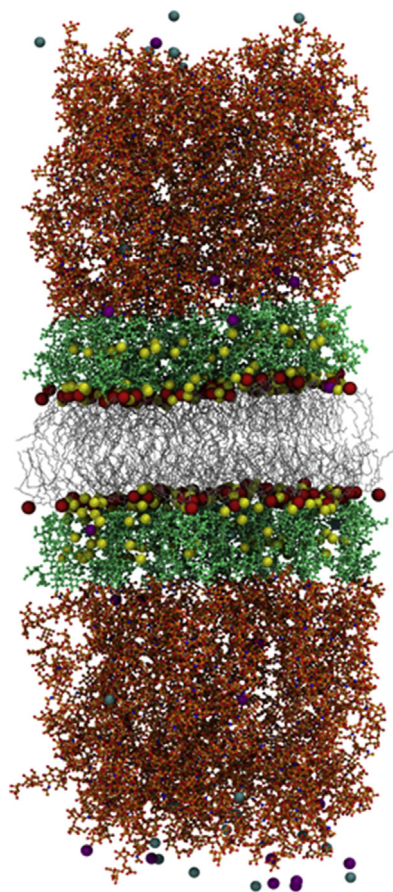

Fig. 2. LPS10 (lipid A, R1 core, and 10 units of the O176 O-antigen) lipid bilayer snapshot at 400 ns. Lipid A is colored gray, the R1 core is colored green, and O-antigen repeating units are colored orange. Phosphate groups are colored red, and calcium, potassium, and chloride ions are shown as yellow, cyan, and purple spheres, respectively. Water molecules are not shown for the sake of clarity.
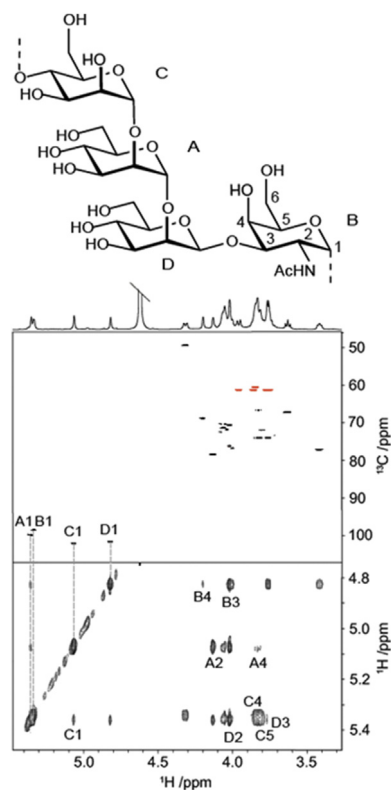
Figure 3. (Top) Schematic structure of the repeating unit of the O-antigen polysaccharide from *E. coli* O176; sugar residues are labeled A – D. (Bottom) Part of ^{1}H,^{13}C-HSQC (10% sparse sampling) and ^{1}H,^{1}H-NOESY (40% sparse sampling, mixing time 180 ms) spectra with selected proton and carbon resonances annotated.

maintain constant temperature with a Langevin coupling coefficient of 1 ps^{-1}, and a Nosé-Hoover Langevin piston (Feller et al., 1995; Martyna et al., 1994) was used to maintain constant pressure with a piston period of 50 fs and a piston decay time of 25 fs. A 2-fs timestep was used for integration together with the SHAKE algorithm (Ryckaert et al., 1977),

where all covalent bonds between hydrogen and the heavy atom were constrained. The van der Waals interactions were smoothly switched off at 10–12 Å by a force-switching function (Steinbach and Brooks, 1994), while the long-range electrostatic interactions were calculated using the particle-mesh Ewald method (Essmann et al., 1995). All the systems (solution and membrane) were simulated with the CHARMM36 (C36) force field for lipids (Klauda et al., 2010), carbohydrates (Patel et al., 2014; Guvench et al., 2008, 2011) and LPS (Jo et al., 2015), and with the TIP3P water model (Jorgensen et al., 1983).

3. Results and discussion

3.1. NMR experiments

The *E. coli* O176 O-antigen polysaccharide consists of tetrasaccharide repeating units (RUs) with the following structure: →4)-α-D-Man*p*-(1 → 2)-α-D-Man*p*-(1 → 2)-β-D-Man*p*-(1 → 3)-α-D-Gal*p*NAc-(1→, where Man*p* corresponds to mannopyranose, and Gal*p*NAc to 2-acetamido-2-deoxy-galactopyranose (Fig. 3). Our previous structural studies using ^{1}H NMR data also determined the chain length of the polysaccharide preparation to be ~10 RUs on average (Olsson et al., 2008). Using 2D NMR experiments, resonance assignments were carried out from ^{1}H,^{13}C-HSQC and ^{1}H,^{1}H-NOESY spectra (Figure S1), which confirmed the structure of the tetrasaccharide RU of the *E. coli* O176 O-antigen.

To investigate the preferred conformation(s) and dynamics of the O-antigen, we set out to measure proton-proton cross-relaxation rates (σ) by ^{1}H,^{1}H-NOESY experiments and to do it not only using conventional uniform sampling (US) but also by a non-uniform sampling (NUS) technique. Traditionally, NMR spectroscopy relies on signal acquisition during a time domain using uniformly sampled data points; higher resolution implies a higher number of data points and thus, a more time-consuming experiment. More recently, the NUS methodology has been developed to allow for the acquisition of a complete spectrum based on significantly fewer data points (Jaravine et al., 2008; Mayzel et al., 2014). Data are recorded using known information or estimates of NMR parameters, such as the magnitude of *J* couplings and T_2 relaxation times, in order to obtain maximum spectral resolution and sensitivity (Kazimierczuk and Orekhov, 2015; Palmer et al., 2015). The information on the various parameter settings will then provide a better distribution of sampling points along the FID during the acquisition. Consequently,

Table 1

US and NUS inter-and intra-glycosidic proton-proton cross-relaxation rates (σ_{US} and σ_{NUS} in s^{-1}) in the *E. coli* O176 polysaccharide derived from PANIC buildup curves, experimentally derived distances (r_{US} and r_{NUS} in Å), and calculated effective proton-proton distances ($r_{Solution}$, r_{LPS5}, r_{LPS10} in Å) from the solution, LPS5, and LPS10 MD simulations as well as $\langle \sigma \cdot r^6_{\text{ref-Solution}} \rangle$ in Å$^6 \cdot$s^{-1}. The standard error (SE) of the slope and R^2 average values for US and NUS cross-relaxation rates are displayed.

Proton pair	σ_{US}	σ_{NUS}	r_{US}[a]	r_{NUS}[a]	$r_{Solution}$	r_{LPS5}	r_{LPS10}
C1-A2	−0.86 ± 0.02	−0.81 ± 0.04	2.41 ± 0.02	2.33 ± 0.04	2.26 ± 0.012	2.26 ± 0.008	2.26 ± 0.007
A1-C1	−0.18 ± 0.02	−0.16 ± 0.02	3.12 ± 0.13	3.05 ± 0.15	3.18 ± 0.082	3.02 ± 0.117	2.90 ± 0.117
A1-D1	−0.24 ± 0.02	−0.19 ± 0.02	2.98 ± 0.07	2.96 ± 0.10	4.35 ± 0.629	4.20 ± 0.055	4.13 ± 0.066
A1-D2	−1.28 ± 0.12	−0.86 ± 0.06	2.25 ± 0.07	2.30 ± 0.05	2.32 ± 0.008	2.32 ± 0.010	2.32 ± 0.016
D1-B3/D2	−2.32 ± 0.24	−1.88 ± 0.23					
D1-B3	−1.57	−1.30	2.18	2.15	2.23 ± 0.005	2.24 ± 0.014	2.24 ± 0.017
D1-B4	−0.16 ± 0.01	−0.09 ± 0.02	3.19 ± 0.08	3.36 ± 0.23	3.43 ± 0.065	3.25 ± 0.142	3.26 ± 0.171
B1–C4/A1-C5	−1.46 ± 0.01	−1.44 ± 0.03					
B1–C4	−0.63	−0.80	2.53	2.33	2.39 ± 0.025	2.31 ± 0.027	2.29 ± 0.042
C1–C2	−0.87 ± 0.03	−0.74 ± 0.06	2.40 ± 0.03	2.36 ± 0.07	2.47 ± 0.001	2.47 ± 0.000	2.47 ± 0.001
A1-A2	−0.60 ± 0.03	−0.52 ± 0.04	2.56 ± 0.05	2.51 ± 0.06	2.46 ± 0.002	2.48 ± 0.003	2.47 ± 0.004
D1-D3	−0.90 ± 0.11	−0.49 ± 0.05	2.39 ± 0.10	2.53 ± 0.09	2.35 ± 0.004	2.34 ± 0.002	2.34 ± 0.003
D1-D5	−0.91 ± 0.14	−0.64 ± 0.06	2.38 ± 0.12	2.42 ± 0.07	2.34 ± 0.002	2.35 ± 0.002	2.34 ± 0.002
B1–B2	−0.76 ± 0.04	−0.68 ± 0.04	2.46 ± 0.05	2.40 ± 0.04	2.40 ± 0.003	2.40 ± 0.002	2.41 ± 0.002
D1-D2	−0.75	−0.58			2.45 ± 0.004	2.45 ± 0.002	2.45 ± 0.002
A1-C5	−0.83	−0.64			2.43 ± 0.028	2.49 ± 0.050	2.55 ± 0.068
$\langle$SE$\rangle$	0.057	0.052					
$\langle R^2 \rangle$	0.90	0.73					
$\langle \sigma_{ref} \cdot r^6_{\text{ref-Solution}} \rangle$	−167.17	−128.90					

[a] Calculated using $r_{ij} = (\langle \sigma_{ref} \cdot r^6_{\text{ref-Solution}} \rangle / \sigma_{ij})^{1/6}$ where the five proton-proton reference distances inside the bracket correspond to C1–C2, A1-A2, D1-D3, D1-D5, and B1–B2 and averaging is carried out over all saved time frames of the two MD simulations for solution (in total 800 ns) while three MD simulations for LPS5 and LPS10 (in total 1.2 µs); separate averaging has been performed for σ from US and NUS NMR data.

fewer data points can be sampled while still maintaining the same resolution, and thus the acquisition time will be reduced accordingly. The NUS approach has been used extensively for protein ^1H and ^{13}C NMR chemical shifts assignment and characterization (Inomata et al., 2009; Miljenović et al., 2017; Sakakibara et al., 2009), and acquisition under NUS conditions has been well established in triple-resonance experiments with a small dynamic range. For instance, the 3D HNCO and HNCOCA spectra of ubiquitin were acquired with only 7% and 6% of the total data set, respectively, from which it was possible to generate good quality spectra (Jaravine et al., 2006); thus, a substantial reduction in acquisition time for the 3D NMR experiments. However, the application in terms of quantification, like for measurement of NOEs, is still challenging due to the high dynamic range (Davies et al., 1985) in $^1H,^1H$-NOESY spectra and for higher dimensionality experiments when NOE-interactions are included as part of the nD NMR experiments (Hyberts et al., 2012).

For the *E. coli* O176 polysaccharide, the sparse sampling technique was first carried out using NUS in a series of $^1H,^{13}C$-HSQC spectra with a decreasing number of acquired points (from 40% to 2% of sparse sampling) and subsequently compared to US (100% of the data points, cf. Figure S1). Besides estimated *J* couplings and T_2 relaxation times, the dispersion of the measured data and the non-linearity in the reconstruction of peaks also have direct or indirect repercussions on the final appearance and signal-to-noise ratio (S/N) of the spectra (Kazimierczuk and Orekhov, 2015; Palmer et al., 2015). Guided by the above and that the number of hypercomplex points should be no less than the number of signals in the spectrum, the 10% NUS $^1H,^{13}C$-HSQC spectrum (Fig. 3) was judged as the best one with respect to spectral quality and S/N in conjunction with time saving of the experiment when performed using the sparse sampling technique.

The $^1H,^1H$-NOE-based conformational analysis of the *E. coli* O176 O-antigen was performed by acquiring phase-sensitive $^1H,^1H$-NOESY experiments with eight mixing times varying from 60 ms to 180 ms employing US and NUS at a coverage level of 40%, similar to the 30% used by Hyberts et al. for 3D ^{15}N-NOESY-HSQC experiments (Hyberts et al., 2012). Herein, we used the time-saving initially obtained by NUS to increase the number of scans by a factor of 2.5, resulting in equal measuring time for both US and NUS experiments, which were performed in quintuplicate to improve the accuracy and reproducibility of the applied methodology. Intra- and inter-residue proton-proton distances were found within and between all residues of the O-antigen (Table 1), and subsequently auto- and cross-peaks in the NOESY spectra were integrated for quantitative analysis.
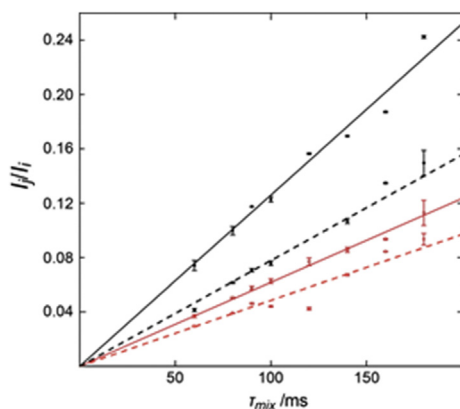

Fig. 4. $^1H,^1H$-NOESY buildup curves of the O-antigen polysaccharide from *E. coli* O176 employing the PANIC approach in which I_j/I_i vs. τ_{mix} are plotted. The cross-relaxation rates, which correspond to $-\sigma_{ij} = I_j/I_i$, are obtained from the slopes of the fitted data; the inter-residue proton pair A1-D2 (solid line) and the intra-residue reference A1-A2 (dashed line) are shown using uniform (black) and non-uniform (red) sampling. Data were plotted with the mean value at each mixing time using in bars the standard error of the mean (SEM) at each point.

Using NOE buildup curves (Widmalm et al., 1992) analyzed by the PANIC approach (Hu and Krishnamurthy, 2006; Macur et al., 1986) (Fig. 4), cross-relaxation rates between proton pairs could be obtained (Table 1). For the PANIC plots, the y-axis intercept was close to zero and ranged from −0.037 to 0.002 for US and from −0.028 to 0.012 for NUS. However, US- and NUS-derived cross-relaxation rates were found slightly different, where the NUS method consistently showed lower values, which may be related to the high dynamic range of NOE measurements. The average standard error of the slope for all σ values was found to be comparable (Table 1), although some difference was observed for the mean R^2 values (0.90 for US and 0.73 for NUS).

Instead of relying on a single reference distance between a pair of protons in one sugar residue in the RUs of the polysaccharide, we herein utilize an approach recently presented and applied to oligosaccharides (Patel et al., 2014). The methodology employs proton-proton distances from MD simulations in an isolated spin-pair approximation (ISPA)
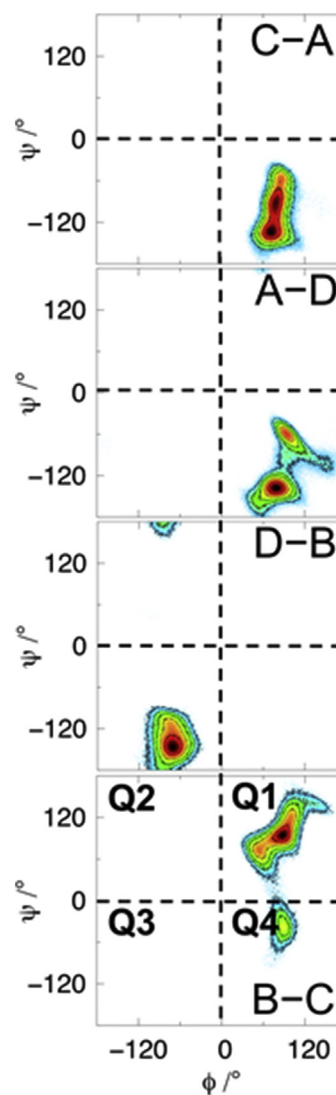

Fig. 5. Two-dimensional free energy surfaces of glycosidic torsion angles ϕ and ψ in the *E. coli* O176 O-antiven polysaccharide from PS10 MD simulations. Free energies are calculated from the natural logarithm of the relative probability and are colored as follows: black for 0 kcal mol^{-1}, red for 0.5 kcal mol^{-1}, yellow for 1.0 kcal mol^{-1}, green for 1.75 kcal mol^{-1}, and blue for 2.5 kcal mol^{-1} The following glycosidic torsion angle definitions were adopted: $\phi = $ O5'–C1'–On–Cn, $\psi = $ C1'–On–Cn–C (n–1), where n is the linkage position.

(Thomas et al., 1991) approach, viz., $r_{ij} = (\langle\sigma_{ref}\cdot r^6_{ref\text{-}Solution}\rangle/\sigma_{ij})^{1/6}$ (Patel et al., 2014); by using proton-proton reference distances inside the bracket calculated over the trajectory, where averaging is carried out over all saved time frames of the MD simulations, effective r_{ij} distances can be obtained. Separate averaging was performed for σ from US and NUS NMR data. When the transglycosidic σ values are applied, the effective inter-nuclear distances derived from US or NUS ^{1}H,^{1}H-NOESY data become highly similar under equal measuring time conditions (Table 1).

3.2. Comparison to MD simulations

The results from the NMR experiments were compared to those calculated from MD simulation trajectories of, in particular, the *E. coli* O176 O-antigen polysaccharide containing 10 RUs (PS10) in solution (Table 1), because this should be highly representative of the polysaccharide preparation used in the NMR experiments; comparisons were also made to the membrane-associated LPS5 and LPS10 having five and ten RUs, respectively. The conformational space sampled by PS10 is described by the two-dimensional free energy surfaces of the glycosidic torsion angles ϕ and ψ (Fig. 5), where the major state of the ϕ torsion angles is present in the *exo*-anomeric conformation (Eklund and Widmalm, 2003; Lemieux and Koto, 1974); notably, the conformational flexibility of the α-linked residues C, A and B occurred along the ψ torsion angle whereas for the β-linked residue D, only a single conformational region was populated (quadrant three). The conformational space was found similar for LPS5 (Figure S2) and LPS10 (Figure S3), although a slightly larger sampling and some changes in populations took place.

The experimentally derived transglycosidic distances showed very good agreement, with differences of ~0.1 Å, to those from the MD simulations of PS10 (Table 1 and Fig. 6), except for the A1-D1 distance between the two anomeric protons that deviates by > 1 Å. However, closer analysis of this proton-proton interaction revealed that the NOE is mediated by the D2 proton at the glycosidic linkage between the two residues (Fig. 7), i.e., a three-spin effect (Widmalm et al., 1992; Dixon et al., 2000) that is highly effective in larger compounds with longer reorientational correlation times like polysaccharides and proteins. The geometry at the most highly populated conformation of PS10, with $\phi = 78°$ and $\psi = -137°$, located in quadrant four of the two-dimensional free energy surface (Fig. 5), is described by $r_{A1\text{-}D1} = 4.58$ Å, $r_{A1\text{-}D2} = 2.30$ Å, $r_{D2\text{-}D1} = 2.44$ Å, and an angle $\theta_{A1\text{-}D2\text{-}D1}$ of 149°, consistent

with the fact that a three-spin effect is operating. The apparent A1-D1 distance from NMR experiment was therefore omitted from further considerations, and instead the effective distance calculated from the MD simulations where $r_{A1\text{-}D1} > 4$ Å was judged as relevant. The use of several proton-proton reference distances makes the analysis less prone to bias, which is also the case when the approach is applied to the NOE data acquired in our previous studies on the *E. coli* O6 (Table S2) and O91 (Table S3) O-antigens (Wu et al., 2013; Blasco et al., 2017). Although the experimentally derived distances are closely similar to those determined previously, they are to be judged with greater credence, because the results do not rely on a single reference distance (and the associated inter-proton dynamics).

Analysis of the conformational preference of α-D-Manp-(1 → 2)-α-D-Manp ($\phi/\psi_{C\text{-}A}$) and α-D-Manp-(1 → 2)-β-D-Manp ($\phi/\psi_{A\text{-}D}$) in the Protein Data Bank (Figure S4) revealed that there is a population distribution of 1441 and 20 glycan structures identified using Glycan Fragment DB (http://glycanstructure.org/fragment-db) (Jo and Im, 2012), very similar to those observed for $\phi/\psi_{C\text{-}A}$ and $\phi/\psi_{A\text{-}D}$ in PS10 (Fig. 5), LPS5 (Figure S2), and LPS10 (Figure S3) simulations. This result suggests that inherent conformational preferences for synperiplanar $\psi_{C\text{-}A}$ and $\psi_{A\text{-}D}$ in solution are also retained in corresponding sugar linkages in LPS5 and LPS10 simulations.

3.3. Structure and dynamics of LPS molecules in a bilayer

Though the conformational sampling of the O176 polysaccharide for contiguous residues, i.e., at the disaccharide level, is similar in solution and LPS systems, small changes in glycosidic linkage torsion angles allow for quite large global conformational changes of the polymeric chain of the PS10 systems when compared to O-antigen part of LPS systems. This is evident from a time-series analysis of end-to-end distance calculations between the first residue of RU1 and last residue of RU10 in PS10 and LPS10 (Fig. 8). Due to availability of free conformational space for PS10, the O-antigen in solution widely varied between extended and curved conformation (Figure S5), which contrasted to the extended polymer chains in LPS systems as a result of close LPS-LPS packing and less available space for movement. Higher dynamical flexibility for the polysaccharide chain PS10 is also observed in solution for the *E. coli* O6 and O91 O-antigens compared to polysaccharide chain in the homogeneous bilayer environment of LPS10 (Fig. 8).
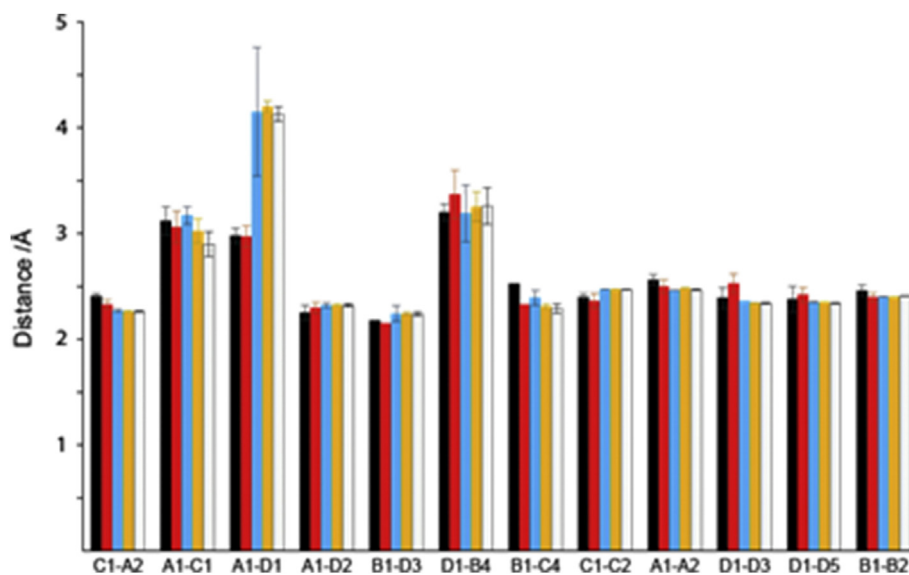

Fig. 6. Bar diagram displaying proton-proton distances in *E. coli* O176 polysaccharide from NMR US (black) and NUS (red), including error bar estimates (SEM) based on cross-relaxation rates, and from MD simulations (solution, LPS5, and LPS10 detailed in blue, orange, and white, respectively).

From the analysis of calculated heavy atom density profiles along the Z-axis (i.e., the membrane normal) for LPS5 and LPS10 bilayer systems, we noticed that the polysaccharide conformational dynamics are further dependent on the polysaccharide molecular length and only to a small extent to type of O-antigen. In general, for all three O-antigens O176, O6, and O91, terminal RUs possess more extensive dynamics with broader density distribution than the residues closer to the outer core which shows narrower density distribution irrespective of bilayer systems (Fig. 9). However, the Z-axis extension of each O-antigen is largely dependent on the O-antigen type. The O176 O-antigen with four linearly-connected sugars in the RU is much less extended in the Z-axis than the *E. coli* O91 O-antigen with five linearly-connected sugars in the RU (Fig. 1). Intere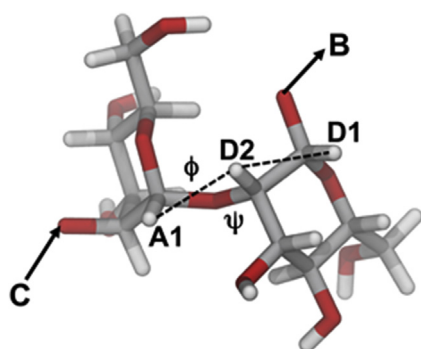stingly, the *E. coli* O6 O-antigen having five sugars with one branch in the RU show the Z-extension in between O176 and O91 O-antigens. In addition, the effect of LPS packing on the dynamics of RUs appears to be slightly different for all three O-antigens with different LPS packing environment. For example, for the O91 O-antigen, the core structures as well as the different RUs in the LPS5 O-antigen are slightly more extended than the corresponding ones in LPS10, but in the case of O6 and O176 RUs, they are less extended in LPS5 compared to LPS10.

Further insight into the impact of O-antigen type on the lipid A packing and dynamics in the LPS5 and LPS10 bilayers was gained from analysis of the area per lipid (APL) and membrane compressibility (Fig. 10). In general, addition of any of O176, O6, and O91 O-antigens increases APL for lipid A groups as compared to APL of lipid A in LPS0 (lipid A + R1 core) bilayer systems. The increased surface area seen in the LPS5 and LPS10 bilayers compared to the LPS0 bilayer may be caused by sterically bulkier O-antigen regions, which push LPS molecules away from each other. Interestingly, this steric effect is the O-antigen length dependent with more influence in LPS5 than LPS10 except the *E. coli* O91 O-antigen for which the negatively charged RUs further push LPS molecules away from each other with more RUs. This non-monotonic trend of APL for O6 and O176 between LPS5 and LPS10 bilayer systems may be related to complex three-dimensional structural arrangements within LPS-LPS interactions with branched O-antigen RUs. Further insight into the membrane dynamics were obtained through the compressibility modulus that can be calculated by $K_A = k_B T$ APL/(N$<\delta$APL$^2>$), where $k_B T$ is the thermal energy and N is the number of lipid A molecules in a leaflet. The K_A in the LPS0 system is ~200 dyn cm^{-1}. For O176 and O6 antigens, LPS5 and LPS10 systems show K_A in the range of 200 dyn cm^{-1}, suggesting little influence of these two O-antigens on membrane dynamics. However, in case of O91, K_A values decrease to 150 dyn/cm in LPS5 and 125 dyn/cm in LPS10 as compared to 200 dyn/cm in LPS0. Decreased in compressibility modulus of the *E. coli* O91 O-antigen LPS can be attributed to LPS-LPS
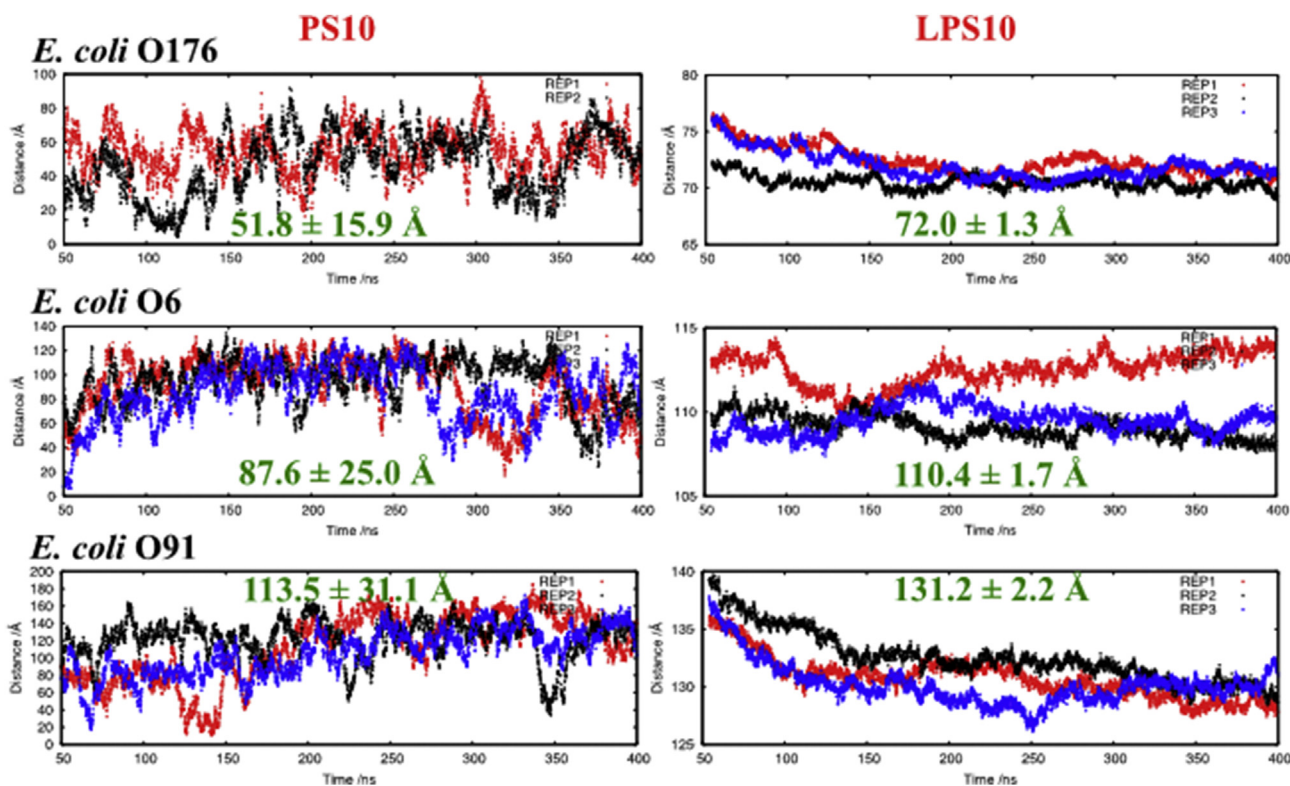

Fig. 7. Molecular model of the most populated conformer ($\phi = 77°$ and $\psi = 136°$) of the A-D disaccharide structural element in the *E. coli* O176 polysaccharide. The effective proton-proton interatomic distances from the MD simulation in this conformational state are: $r_{A1-D2} = 2.30$ Å, $r_{D2-D1} = 2.44$ Å, and $r_{A1-D1} = 4.58$ Å; the average angle $\theta_{A1-D2-D1} = 149°$.

Fig. 8. Time-series of the end-to-end distances in *E. coli* O176, O6, and O91 antigens between first residue of RU1 and last residue of RU10 in LPS10 bilayers and PS10 solution with the average distance and the standard errors over three independent simulations (replicas).
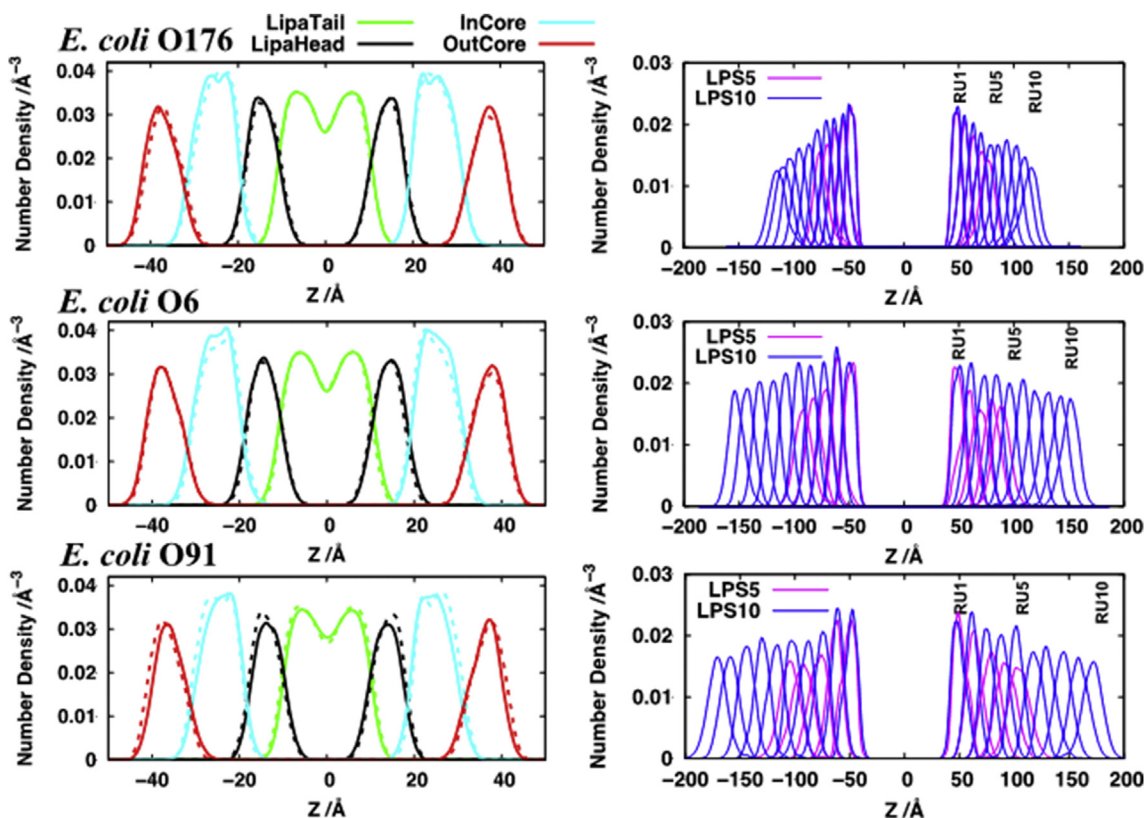
Figure 9. (Left) Heavy atom density profiles along the Z-axis (i.e., the membrane normal) for lipid A acyl chains (LipaTail), lipid A headgroups (LipaHead), inner core sugars (InCore), and outer core sugars (OutCore) for all three O-antigens O176, O6 and O91. Solid and dotted lines correspond to LPS10 and LPS5 bilayers, respectively. (Right) Comparison of dynamics of O-antigen repeating units RU1 − RU5 in the LPS5 bilayers and RU1 − RU10 in the LPS10 bilayers.
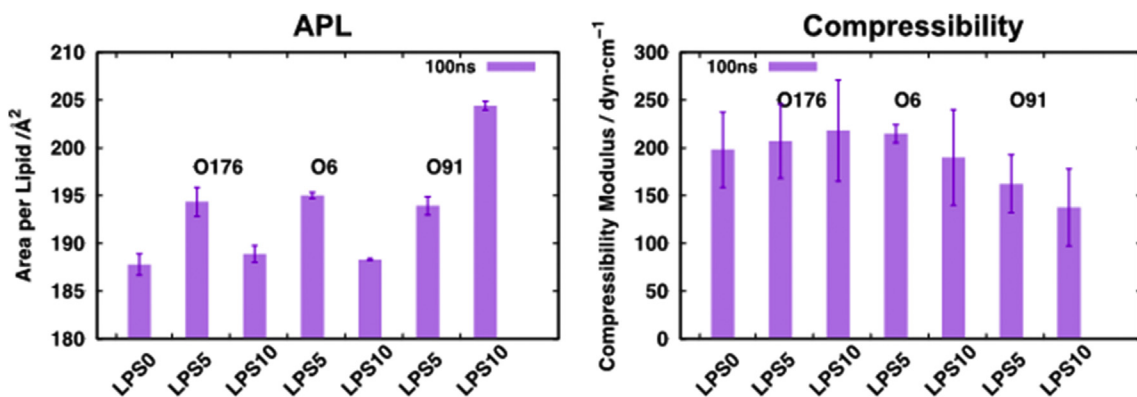

Fig. 10. Average lipid bilayer properties, area per lipid (APL) and compressibility modulus, over the last 100 ns for the homogeneous LPS bilayers, without O-antigen LPS0 and with O-antigens (O176, O6 and O91) LPS5 and LPS10 with three independent systems for all.
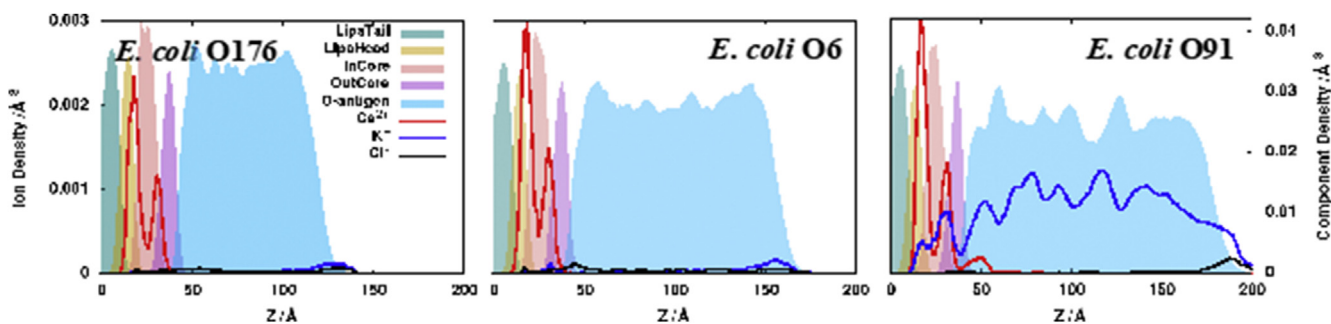

Fig. 11. Distributions of ions (Ca^{2+}, K^{2+}, and Cl^{-}) along the Z-axis (i.e., the membrane normal), mapping onto the heavy atom density profiles of different LPS components in the *E. coli* O176, O6, and O91 LPS10 bilayer systems. Only the $Z > 0$ membrane portion is shown after symmetrization. K^{+} and Cl^{-} ion densities were scaled by a factor of two, for the sake of clarity.

repulsion due to the negatively charged O-antigen, making the LPS bilayer easier to be compressed (i.e., more fluctuations around the bilayer average area).

In addition, net negative charge of the O91 polysaccharide compared to neutral charge of the O176 and O6 O-antigens appears to influence overall distribution of ions in respective systems and affect packing and dynamics of LPS. Different distribution patterns of ions particularly for K^+ ions are clearly observed with calculated ion density profiles along the Z-axis (Fig. 11). The negatively charged O91 O-antigen facilitates deep penetration of K^+ ions, while this did not take place for neutral charge of O176 and O6 polysaccharides. This penetration of K^+ ions along the O91 O-antigen allows their interaction with the head group of lipid A in the LPS bilayer and leads to competition with Ca^{2+} ions and makes lipid A packing more compressible. Importantly, our previous study of lipid A bilayer systems from different bacterial species indicated that lipid A with monovalent cations (K^+ or Na^+) is more compressible than Ca^{2+} neutralized lipid A (Kim et al., 2016).

4. Conclusions

In summary, this work provides insight into the conformational preferences of the *E. coli* O176 O-antigen polysaccharide in solution and the full LPS in a membrane model. The effective transglycosidic proton-proton distances in the polysaccharide derived from NMR experiments showed very good agreement to those from MD simulations using the polysaccharide and LPS bilayers as well. Moreover, even though the NMR cross-relaxation rates derived using a non-uniform sampling technique were consistently lower, we observed that when these rates were translated into effective internuclear distances, the distances became highly similar to those from conventional uniform sampling, under equal measuring time conditions. Like for the *E. coli* O176 O-antigen, additional MD simulations of the LPS and the polysaccharide were performed and analyzed for *E. coli* O6 and O91. The same approach, in which several intra-residual proton-proton interactions were used as reference to calculate transglycosidic distances, gives higher credence to the derived effective distances for *E. coli* O6 and O91 polysaccharides. Conformational sampling of the O176 polysaccharide in solution and LPS systems is quite similar at the disaccharide level, but the polymeric chain of PS10 is very flexible compared to O-antigen part of LPS systems as a result of close LPS-LPS packing and less available space for movement. Moreover, overall O-antigen charges also play important role in LPS-LPS packing and dynamics as evident from the area per lipid and compressibility modulus analysis. This suggests significant decrease in membrane compressibility modulus for LPS systems with the negatively charged O91 O-antigen compared to neutral O176 and O6 LPS systems. In addition, the similarities between the O-antigen on its own and as a constituent of the full LPS in bilayer environment makes it possible to realistically describe the LPS conformation and dynamics from the MD simulations.

Declaration of Competing Interest

None.

CRediT authorship contribution statement

Dhilon S. Patel: Methodology, Validation, Formal analysis, Investigation, Data curation, Writing - original draft, Writing - review & editing. **Pilar Blasco:** Methodology, Validation, Formal analysis, Investigation, Data curation, Writing - original draft, Writing - review & editing. **Göran Widmalm:** Conceptualization, Methodology, Resources, Writing - original draft, Writing - review & editing, Supervision. **Wonpil Im:** Conceptualization, Methodology, Resources, Writing - review & editing, Supervision.

Appendix A. Supplementary data

Supplementary data to this article can be found online at https://doi.org/10.1016/j.crstbi.2020.04.004.

References

Alexander, C., Rietschel, E.T., 2001. Bacterial lipopolysaccharides and innate immunity. J. Endotoxin Res. 7, 167–202. https://doi.org/10.1177/09680519010070030101.

Andersen, H.C., 1980. Molecular dynamics simulations at constant pressure and/or temperature. J. Chem. Phys. 72, 2384–2393. https://doi.org/10.1063/1.439486.

Blasco, P., Patel, D.S., Engström, O., Im, W., Widmalm, G., 2017. Conformational synamics of the lipopolysaccharide from *Escherichia coli* O91 revealed by nuclear magnetic resonance spectroscopy and molecular simulations. Biochemistry 56, 3826–3839. https://doi.org/10.1021/acs.biochem.7b00106.

Boutet, J., Blasco, P., Guerreiro, C., Thouron, F., Dartevelle, S., Nato, F., Cañada, F.J., Ardá, A., Phalipon, A., Jiménez-Barbero, J., Mulard, L.A., 2016. Detailed investigation of the immunodominant role of O-antigen stoichiometric O-acetylation as revealed by chemical synthesis, immunochemistry, solution conformation and STD-NMR spectroscopy for *Shigella flexneri*. Chem. Eur J. 22, 10892–10911. https://doi.org/10.1002/chem.201600567.

Brooks, B.R., Brooks, C.L., Mackerell, A.D., Nilsson, L., Petrella, R.J., Roux, B., Won, Y., Archontis, G., Bartels, C., Boresch, S., Caflisch, A., Caves, L., Cui, Q., Dinner, A.R., Feig, M., Fischer, S., Gao, J., Hodoscek, M., Im, W., Kuczera, K., Lazaridis, T., Ma, J., Ovchinnikov, V., Paci, E., Pastor, R.W., Post, C.B., Pu, J.Z., Schaefer, M., Tidor, B., Venable, R.M., Woodcock, H.L., Wu, X., Yang, W., York, D.M., Karplus, M., 2009. CHARMM: the biomolecular simulation program. J. Comput. Chem. 30, 1545–1614. https://doi.org/10.1002/jcc.21287.

Davies, S., Bauer, C., Barker, P., Freeman, R., 1985. The dynamic range problem in NMR. J. Magn. Reson. 64, 155–159. https://doi.org/10.1016/0022-2364(85)90045-9.

Dixon, A.M., Widmalm, G., Bull, T.E., 2000. Modified GOESY in the analysis of disaccharide conformation. J. Magn. Reson. 147, 266–272. https://doi.org/10.1006/jmre.2000.2211.

Efron, B., Stein, C., 1981. The jackknife estimate of variance. Ann. Stat. 9, 586–596.

Eklund, R., Widmalm, G., 2003. Molecular dynamics simulations of an oligosaccharide using a force field modified for carbohydrates. Carbohydr. Res. 338, 393–398. https://doi.org/10.1016/S0008-6215(02)00503-7.

Enkavi, G., Javanainen, M., Kulig, W., Róg, T., Vattulainen, I., 2019. Multiscale simulations of biological membranes: the challenge to understand biological phenomena in a living substance. Chem. Rev. 119, 5607–5774. https://doi.org/10.1021/acs.chemrev.8b00538.

Essmann, U., Perera, L., Berkowitz, M.L., Darden, T., Lee, H., Pedersen, L.G., 1995. A smooth particle mesh Ewald method. J. Chem. Phys. 103, 8577–8593. https://doi.org/10.1063/1.470117.

Feizi, T., Mulloy, B., 2003. Carbohydrates and glycoconjugates. Glycomics: the new era of carbohydrate biology. Curr. Opin. Struct. Biol. 13, 602–604. https://doi.org/10.1016/j.sbi.2003.09.001.

Feller, S.E., Zhang, Y., Pastor, R.W., Brooks, B.R., 1995. Constant pressure molecular dynamics simulation: the Langevin piston method. J. Chem. Phys. 103, 4613–4621. https://doi.org/10.1063/1.470648.

Findeisen, M., Brand, T., Berger, S., 2007. A 1H-NMR thermometer suitable for cryoprobes. Magn. Reson. Chem. 45, 175–178. https://doi.org/10.1002/mrc.1941.

Guvench, O., Greene, S.N., Kamath, G., Brady, J.W., Venable, R.M., Pastor, R.W., Mackerell, A.D., 2008. Additive empirical force field for hexopyranose monosaccharides. J. Comput. Chem. 29, 2543–2564. https://doi.org/10.1002/jcc.21004.

Guvench, O., Hatcher, E., Venable, R.M., Pastor, R.W., MacKerell, A.D., 2009. CHARMM additive all-atom force field for glycosidic linkages between hexopyranoses. J. Chem. Theor. Comput. 5, 2353–2370. https://doi.org/10.1021/ct900242e.

Guvench, O., Mallajosyula, S.S., Raman, E.P., Hatcher, E., Vanommeslaeghe, K., Foster, T.J., Jamison, F.W., MacKerell, A.D., 2011. CHARMM additive all-atom force field for carbohydrate derivatives and its utility in polysaccharide and carbohydrate–protein modeling. J. Chem. Theor. Comput. 7, 3162–3180. https://doi.org/10.1021/ct200328p.

Hoover, W.G., 1985. Canonical dynamics: equilibrium phase-space distributions. Phys. Rev. 31, 1695–1697. https://doi.org/10.1103/physreva.31.1695.

Hu, H., Krishnamurthy, K., 2006. Revisiting the initial rate approximation in kinetic NOE measurements. J. Magn. Reson. 182, 173–177. https://doi.org/10.1016/j.jmr.2006.06.009.

Hyberts, S.G., Arthanari, H., Wagner, G., 2012. Applications of non-uniform sampling and processing. Top. Curr. Chem. 316, 125–148. https://doi.org/10.1007/128_2011_187.

Inomata, K., Ohno, A., Tochio, H., Isogai, S., Tenno, T., Nakase, I., Takeuchi, T., Futaki, S., Ito, Y., Hiroaki, H., Shirakawa, M., 2009. High-resolution multi-dimensional NMR spectroscopy of proteins in human cells. Nature 458, 106–109. https://doi.org/10.1038/nature07839.

Jaravine, V., Ibraghimov, I., Orekhov, V.Y., 2006. Removal of a time barrier for high-resolution multidimensional NMR spectroscopy. Nat. Methods 3, 605–607. https://doi.org/10.1038/nmeth900.

Jaravine, V.a., Zhuravleva, A.V., Permi, P., Ibraghimov, I., Orekhov, V.Y., 2008. Hyperdimensional NMR spectroscopy with nonlinear sampling. J. Am. Chem. Soc. 130, 3927–3936. https://doi.org/10.1021/ja077282o.

Jo, S., Im, W., 2012. Glycan fragment database: a database of PDB-based glycan 3D structures. Nucleic Acids Res. 41, D470–D474. https://doi.org/10.1093/nar/gks987. Available at: http://www.glycanstructure.org.

Jo, S., Kim, T., Im, W., 2007. Automated builder and database of protein/membrane complexes for molecular dynamics simulations. PloS One 2, e880. https://doi.org/10.1371/journal.pone.0000880.

Jo, S., Kim, T., Iyer, V.G., Im, W., 2008. CHARMM-GUI: a web-based graphical user interface for CHARMM. J. Comput. Chem. 29, 1859–1865. https://doi.org/10.1002/jcc.20945.

Jo, S., Lim, J.B., Klauda, J.B., Im, W., 2009. CHARMM-GUI membrane builder for mixed bilayers and its application to yeast membranes. Biophys. J. 97, 50–58. https://doi.org/10.1016/j.bpj.2009.04.013.

Jo, S., Song, K.C., Desaire, H., MacKerell, A.D., Im, W., 2011. Glycan reader: automated sugar identification and simulation preparation for carbohydrates and glycoproteins. J. Comput. Chem. 32, 3135–3141. https://doi.org/10.1002/jcc.21886.

Jo, S., Wu, E.L., Stuhlsatz, D., Klauda, J.B., MacKerell, A.D., Widmalm, G., Im, W., 2015. In: Lütteke, T., Frank, M. (Eds.), Lipopolysaccharide Membrane Building and Simulation. Glycoinformatics, vol. 1273. Springer, New York, New York, NY, pp. 391–406.

Jorgensen, W.L., Chandrasekhar, J., Madura, J.D., Impey, R.W., Klein, M.L., 1983. Comparison of simple potential functions for simulating liquid water. J. Chem. Phys. 79, 926–935. https://doi.org/10.1063/1.445869.

Kazimierczuk, K., Orekhov, V.Y., 2011. Accelerated NMR spectroscopy by using compressed sensing. Angew. Chem. Int. Ed. 50, 5556–5559. https://doi.org/10.1002/anie.201100370.

Kazimierczuk, K., Orekhov, V., 2015. Non-uniform sampling: post-fourier era of NMR data collection and processing. Magn. Reson. Chem. 53, 921–926. https://doi.org/10.1002/mrc.4284.

Kim, S., Patel, D.S., Park, S., Slusky, J., Klauda, Jeffery B., Widmalm, G., Im, W., 2016. Bilayer properties of lipid A from various Gram-negative bacteria. Biophys. J. 111, 1750–1760. https://doi.org/10.1016/j.bpj.2016.09.001.

Klauda, J.B., Venable, R.M., Freites, J.A., O'Connor, J.W., Tobias, D.J., Mondragon-Ramirez, C., Vorobyov, I., MacKerell, A.D., Pastor, R.W., 2010. Update of the CHARMM all-atom additive force field for lipids: validation on six lipid types. J. Phys. Chem. B 114, 7830–7843. https://doi.org/10.1021/jp101759q.

Landersjö, C., Jansson, J.L.M., Maliniak, A., Widmalm, G., 2005. Conformational analysis of a tetrasaccharide based on NMR spectroscopy and molecular dynamics simulations. J. Phys. Chem. B 109, 17320–17326. https://doi.org/10.1021/jp052206y.

Lee, J., Cheng, X., Swails, J.M., Yeom, M.S., Eastman, P.K., Lemkul, J.A., Wei, S., Buckner, J., Jeong, J.C., Qi, Y., Jo, S., Pande, V.S., Case, D.A., Brooks 3rd, C.L., MacKerell Jr., A.D., Klauda, J.B., Im, W., 2016. CHARMM-GUI input generator for NAMD, GROMACS, AMBER, OpenMM, and CHARMM/OpenMM simulations using the CHARMM36 additive force field. J. Chem. Theor. Comput. 12, 405–413. https://doi.org/10.1021/acs.jctc.5b00935.

Lee, J., Patel, D.S., Ståhle, J., Park, S.-J., Kern, N.R., Kim, S., Lee, J., Cheng, X., Valvano, M.A., Holst, O., Knirel, Y.A., Qi, Y., Jo, S., Klauda, J.B., Widmalm, G., Im, W., 2019. CHARMM-GUI membrane builder for complex biological membrane simulations with glycolipids and lipoglycans. J. Chem. Theor. Comput. 15, 775–786. https://doi.org/10.1021/acs.jctc.8b01066.

Lemieux, R.U., Koto, S., 1974. The conformational properties of glycosidic linkages. Tetrahedron 30, 1933–1944. https://doi.org/10.1016/S0040-4020(01)97324-7.

Macur, S., Farmer, B.T., Brown, L.R., 1986. An improved method for the determination of cross-relaxation rates from NOE data. J. Magn. Reson. 70, 493–499. https://doi.org/10.1016/0022-2364(86)90143-5.

Martyna, G.J., Tobias, D.J., Klein, M.L., 1994. Constant pressure molecular dynamics algorithms. J. Chem. Phys. 101, 4177–4189. https://doi.org/10.1063/1.467468.

Mayzel, M., Rosenlöw, J., Isaksson, L., Orekhov, V.Y., 2014. Time-resolved multidimensional NMR with non-uniform sampling. J. Biomol. NMR 58, 129–139. https://doi.org/10.1007/s10858-013-9811-1.

Miljenović, T., Jia, X., Lavrencic, P., Kobe, B., Mobli, M., 2017. A non-uniform sampling approach enables studies of dilute and unstable proteins. J. Biomol. NMR 68, 119–127. https://doi.org/10.1007/s10858-017-0091-z.

Mobli, M., Maciejewski, M.W., Schuyler, A.D., Stern, A.S., Hoch, J.C., 2012. Sparse sampling methods in multidimensional NMR. Phys. Chem. Chem. Phys. 14, 10835–10843. https://doi.org/10.1039/C2CP40174F.

Nosé, S., Klein, M.L., 1983. A study of solid and liquid carbon tetrafluoride using the constant pressure molecular dynamics technique. J. Chem. Phys. 78, 6928–6939. https://doi.org/10.1063/1.444641.

Olsson, U., Weintraub, A., Widmalm, G., 2008. Structural determination of the O-antigenic polysaccharide from the verocytotoxin-producing *Escherichia coli* O176. Carbohydr. Res. 343, 805–809. https://doi.org/10.1016/j.carres.2008.01.003.

Orekhov, V.Y., Jaravine, V.a., 2011. Analysis of non-uniformly sampled spectra with multi-dimensional decomposition. Prog. Nucl. Magn. Reson. Spectrosc. 59, 271–292. https://doi.org/10.1016/j.pnmrs.2011.02.002.

Palmer, M.R., Suiter, C.L., Henry, G.E., Rovnyak, J., Hoch, J.C., Polenova, T., Rovnyak, D., 2015. Sensitivity of nonuniform sampling NMR. J. Phys. Chem. B 119, 6502–6515. https://doi.org/10.1021/jp5126415.

Park, S.-J., Lee, J., Qi, Y., Kern, N.R., Lee, H.S., Jo, S., Joung, I., Joo, K., Lee, J., Im, W., 2019. CHARMM-GUI *Glycan Modeler* for modeling and simulation of carbohydrates and glycoconjugates. Glycobiology 29, 320–331. https://doi.org/10.1093/glycob/cwz003.

Patel, D.S., Pendrill, R., Mallajosyula, S.S., Widmalm, G., MacKerell, A.D., 2014. Conformational properties of α- or β-(1→6)-linked oligosaccharides: Hamiltonian replica exchange MD simulations and NMR experiments. J. Phys. Chem. B 118, 2851–2871. https://doi.org/10.1021/jp412051v.

Patel, D.S., Re, S., Wu, E.L., Qi, Y., Klebba, P.E., Widmalm, G., Yeom, M.S., Sugita, Y., Im, W., 2016. Dynamics and interactions of OmpF and LPS: influence on pore accessibility and ion permeability. Biophys. J. 110, 930–938. https://doi.org/10.1016/j.bpj.2016.01.002.

Pendrill, R., Säwén, E., Widmalm, G., 2013. Conformation and dynamics at a flexible glycosidic linkage revealed by NMR spectroscopy and molecular dynamics simulations: analysis of β-L-Fucp-(1→6)-α-D-Glcp-OMe in water solution. J. Phys. Chem. B 117, 14709–14722. https://doi.org/10.1021/jp409985h.

Phillips, J.C., Braun, R., Wang, W., Gumbart, J., Tajkhorshid, E., Villa, E., Chipot, C., Skeel, R.D., Kalé, L., Schulten, K., 2005. Scalable molecular dynamics with NAMD. J. Comput. Chem. 26, 1781–1802. https://doi.org/10.1002/jcc.20289.

Prestegard, J.H., Liu, J., Widmalm, G., 2015. Oligosaccharides and polysaccharides. Essentials of glycobiology. In: third ed. Cold Spring Harbor Laboratory Press., NY, pp. 31–40.

Rietschel, E.T., Kirikae, T., Schade, F.U., Mamat, U., Schmidt, G., Loppnow, H., Ulmer, A.J., Zähringer, U., Seydel, U., Di Padova, F., 1994. Bacterial endotoxin: molecular relationships of structure to activity and function. Faseb. J. 8, 217–225. https://doi.org/10.1096/fasebj.8.2.8119492.

Ryckaert, J.-P., Ciccotti, G., Berendsen, H.J.C., 1977. Numerical integration of the cartesian equations of motion of a system with constraints: molecular dynamics of n-alkanes. J. Comput. Phys. 23, 327–341. https://doi.org/10.1016/0021-9991(77)90098-5.

Sakakibara, D., Sasaki, A., Ikeya, T., Hamatsu, J., Hanashima, T., Mishima, M., Yoshimasu, M., Hayashi, N., Mikawa, T., Wälchli, M., Smith, B.O., Shirakawa, M., Güntert, P., Ito, Y., 2009. Protein structure determination in living cells by in-cell NMR spectroscopy. Nature 458, 102–105. https://doi.org/10.1038/nature07814.

Ståhle, J., Widmalm, G., 2019. Lipopolysaccharides of Gram-negative bacteria: biosynthesis and structural aspects. Trends Glycosci. Glycotechnol. 31, E159–E171. https://doi.org/10.4052/tigg.1749.7E.

Steinbach, P.J., Brooks, B.R., 1994. New spherical-cutoff methods for long-range forces in macromolecular simulation. J. Comput. Chem. 15, 667–683. https://doi.org/10.1002/jcc.540150702.

Stenutz, R., Weintraub, A., Widmalm, G., 2006. The structures of *Escherichia coli* O-polysaccharide antigens. FEMS Microbiol. Rev. 30, 382–403. https://doi.org/10.1111/j.1574-6976.2006.00016.x.

Thomas, P.D., Basus, V.J., James, T.L., 1991. Protein solution structure determination using distances from two-dimensional nuclear Overhauser effect experiments: effect of approximations on the accuracy of derived structures. Proc. Natl. Acad. Sci. U.S.A. 88, 1237–1241. https://doi.org/10.1073/pnas.88.4.1237.

Thrippleton, M.J., Keeler, J., 2003. Elimination of zero-quantum interference in two-dimensional NMR spectra. Angew. Chem. Int. Ed. 42, 3938–3941. https://doi.org/10.1002/anie.200351947.

Varki, A., 2017. Biological roles of glycans. Glycobiology 27, 3–49. https://doi.org/10.1093/glycob/cww086.

Wade, L.G., 1999. Organic Chemistry. Prentice-Hall, Inc.

Widmalm, G., Byrd, R.A., Egan, W., 1992. A conformation study of α-L-rhap-(1 → 2)-α-Lrhap-(1 → OMe) by NMR nuclear overhauser effect spectroscopy (NOESY) and molecular dynamics calculations. Carbohydr. Res. 229, 195–211. https://doi.org/10.1016/S0008-6215(00)90570-6.

Woods, R.J., 2018. Predicting the structures of glycans, glycoproteins, and their complexes. Chem. Rev. 118, 8005–8024. https://doi.org/10.1021/acs.chemrev.8b00032.

Wu, E.L., Engström, O., Jo, S., Stuhlsatz, D., Yeom, Min S., Klauda, J.B., Widmalm, G., Im, W., 2013. Molecular dynamics and NMR spectroscopy studies of E. coli lipopolysaccharide structure and dynamics. Biophys. J. 105, 1444–1455. https://doi.org/10.1016/j.bpj.2013.08.002.

Wu, E.L., Cheng, X., Jo, S., Rui, H., Song, K.C., Dávila-Contreras, E.M., Qi, Y., Lee, J., Monje-Galvan, V., Venable, R.M., Klauda, J.B., Im, W., 2014a. CHARMM-GUI *Membrane Builder* toward realistic biological membrane simulations. J. Comput. Chem. 35, 1997–2004. https://doi.org/10.1002/jcc.23702.

Wu, E.L., Fleming, P.J., Yeom, M.S., Widmalm, G., Klauda, J.B., Fleming, K.G., Im, W., 2014b. E. coli outer membrane and interactions with OmpLA. Biophys. J. 106, 2493–2502. https://doi.org/10.1016/j.bpj.2014.04.024.